Appl Nanosci (2016) 6:1059–1064
DOI 10.1007/s13204-015-0515-6

ORIGINAL ARTICLE

Structural investigation of nanomixed $xSnO_2$–Al_2O_3 synthesized by sol–gel route

C. Kumar[1] · N. K. Mishra[1] · A. Kumar[1,2] · M. Bhatt[1] · P. Chaudhary[3] · R. Singh[1]

Received: 23 November 2015 / Accepted: 11 December 2015 / Published online: 31 December 2015

Abstract Nanomixed SnO_2–Al_2O_3 with variable composition has been synthesized by sol–gel technique using aluminium dichloride and stannous chloride as precursors. Synthesized nanocomposites have been characterized using various techniques such as X-ray diffraction (XRD), Fourier transform infrared, scanning electron microscopy and Energy-dispersive X-ray spectroscopy (EDX), Brunauer–Emmett–Teller (BET). XRD shows decrease in crystallinity as alumina component increases in following series of nanomixed oxides. The specific surface area calculated by Brunauer–Emmett–Teller (BET) method was about 191 m^2/g and average pore diameter of 158 Å.

Keywords Nanomixed · Alumina · Cystallinity · Sol–gel

Introduction

The advancement in nanoscience can be attributed to its wide range of properties and applications (Mandayo 2007). SnO_2 is an important n-type wide-energy-gap (E_g = 3.64 eV, 330 K) which makes it more valuable in solid state gas sensors (Buttà et al. 1992; Ying et al. 2004), transparent conducting electrodes (Chopra et al. 1983), rechargeable Li batteries (Peng et al. 2000) and optical electronic devices (Aoki and Sasakur 1970). Physical properties like electrical, catalytic, etc. can be enhanced considerably by mixing of oxides. Characterization of some mixed-metal oxides with excellent properties has been reported (Kirszensztej et al. 2004; Lopez et al. 1992; Lin et al. 1997; Sheng et al. 1994). Saha et al. (2001) reported that addition of alumina to SnO_2 can improve the properties of SnO_2 sensors, even without altering the lattice of SnO_2. Best electro-chemical performance is achieved while applying Al-doped SnO_2 composites as the active anode material, and the electrochemical performance of 10 % Al-containing SnO_2 is strongly influenced by the precursors and thermal treatment (Alcantara et al. 2000). Alumina doping in range of 5 % can enhance the gas sensitivity of SnO_2 towards hydrogen (Xu et al. 1991), exhibit efficient applications in display devices and vacuum electronics (Ma et al. 2008). SnO_2 and Al_2O_3 give the best capacitive performance with a value of 119 F g^{-1} after being cycled 1000 times in comparison with the pure SnO_2 (Jayalakshmi et al. 2006; Venugopal et al. 2008), shows excellent catalytic effect (Adriana et al. 2008). Al_2O_3 can also be used as a binder in SnO_2 sensors (Yamazoe 1991; Nakamura 1989). Various methods have been used for preparing mixed metal oxides. Among these techniques, sol–gel has proved to be simple, reproducible and inexpensive route for large area of applications and are of particular interest for generating materials intermixed almost at the atomic level. Due to its ability to bring several components into solution phase during the sol–gel step makes this technique attractive for the preparation of multi-component oxides (Heiba et al. 2010). In this present work, mixed metal oxide of SnO_2–Al_2O_3 of variable composition has been synthesized by using sol–gel technique and characterized for their structural and microstructural properties.

✉ R. Singh
rajeev@arsd.du.ac.in

[1] Material/Organometallics Laboratory, Department of Chemistry, Atma Ram Sanatan Dharma College, University of Delhi, Dhaula Kuan, New Delhi 110 021, New Delhi, India

[2] Department of Polymer Science, Bhaskaracharya College of Applied Sciences, University of Delhi, Dwarka, New Delhi 110075, New Delhi, India

[3] Department of Chemistry, Maitreyi College, University of Delhi, Bapudham Complex, Chanakyapuri, New Delhi 110021, New Delhi, India

Materials and methods

$SnCl_2{\cdot}2H_2O$ (97 % purity) and aqueous ammonia (28–30 %/14.8 M) were purchased commercially from Molychem. $AlCl_3$ was purchased from Thomas Baker (99.5 % purity). Series of nanomixed SnO_2-Al_2O_3 have been synthesized by varying the Al to Sn molar ratio in the order 1:0, 2:1, 1:1, 1:2, 0:1. Ethanolic solution of aluminium trichloride ($AlCl_3$) was added to an ethanolic solution of stannous chloride dihydrate ($SnCl_2{\cdot}2H_2O$) under vigorous stirring, which resulted in the formation of a transparent sol. Thereafter an amount of nearly 7–8 ml aqueous ammonia solution was added dropwise to the above solution under constant stirring in a controlled manner till the formation of a gel. The resulting gel was filtered and washed with methanol to remove impurities, and subsequently dried at 100°C for 2 h in order to obtain dried gel. Thus dried gel was further calcined at 450°C for 4 h at 5 °C per minute rate of increase of temperature and the calcined powder was crushed to fineness using mortar and pestle.

To identify phases and their crystallinity, powder X-ray diffraction (XRD) studies were carried out by Advance Rigaku diffractometer using CuKα (λ=0.15406 nm), radiation in the 2θ range from 10 to 80°. The scanning electron microscopy (SEM) images were recorded on JEOL JSM 6610V and used to investigate the morphology and the particle size of the product. EDX was carried out on Zeiss EDAX EVO-18 at 15k Volt. Microscopic images were obtained using a TEM TECHNAI GT30 50–300 with was operated at 80 kV. FTIR spectra have been recorded on Perkin Elmer 5700 in transmission mode in the wavenumber range 400–4000 cm^{-1}. The spectroscopic grade KBr pellets were used for collecting the spectra with a resolution of 4 cm^{-1} performing 32 scans. The nitrogen adsorption–desorption isotherms were measured at 77 K using Quantachrome Autosorb Automated Gas Sorption System The samples were degassed at 200 °C for 3 h under vacuum before measurement. The specific surface areas were calculated by Brunauer–Emmett–Teller (BET) method. The pore diameter and pore size distribution were measured from desorption branches by the Barrett–Joyner–Halenda (BJH) method.

Result and discussion

The phase purity of nanomixed $xSnO_2$–Al_2O_3 was studied by powder X-ray diffraction (XRD) patterns as shown in the Fig. 1. Miller indices (hkl) of the diffraction peaks of SnO_2–Al_2O_3 nanocomposites are matched with JCPDS card numbers 41–1445 and 010–0425. The peak broadening in the XRD pattern indicates that the particles are nanosized with size ranging between 13 and 15 nm which has been estimated from the Debye–Scherrer's equation using the XRD line broadening as follows

$$\beta = k\lambda/s\cos\theta \quad (1)$$

where s is the crystallite size, λ is the wavelength of the X-ray radiation (Cu K= 0.15406 nm), k constant taken as 0.94, θ the diffraction angle and β is the line full width at half maximum height.

Powder XRD patterns confirm that there is no appearance of any impurity peaks in the nanocomposites. The XRD patterns of the system $xSnO_2$–Al_2O_3 with x = 0, 25, 50, 75, 100 % calcined at 450 °C are shown in Fig. 1. XRD graph contains remarkable peak broadening for the doped samples with alumina compared with pure SnO_2, representing that incorporation of alumina can efficiently inhibit crytallinity of SnO_2 throughout the process of calcinations. Figure 1 also shows that the diffraction peaks become narrower and stronger for pure SnO_2 revealing that the crystallites grow larger and the crystallinity is improved. Diffraction patterns of the doped samples bear a resemblance to that of the pure SnO_2 excluding some peaks which belongs to Al_2O_3. This means that Aluminium is entrenched in the SnO_2 lattice, interstitially forming a solid solution (Heiba et al. 2010). Decrease in crystallite size and crystallinity were observed with the increase in doping amount of aluminium in SnO_2 lattice was observed (Fig. 2; Table 1).

The comparative FTIR spectrum for all the five synthesized nanocomposites is shown in Fig. 3. Spectra of each sample shows a well-defined peaks around 620–600 cm^{-1} which can be attributed to Sn–O or Sn=O bond stretching (Niranjan et al. 2005; Granquist 1990). Broad peak around 3500–3400 cm^{-1} is due to presence of moisture in the samples. Broadening of Sn–O bond peak in sample with increasing percentage of aluminium can be attributed to formation of Sn–O–Al bond, which shows the formation of mixed metal oxide nanoparticles.

Nitrogen adsorption isotherms of 0.5 SnO_2–0.5Al_2O_3 was plotted (Fig. 4) which resembles with isotherm of type IV according to the IUPAC nomenclature (Sing et al.1985). This generally occurs on porous adsorbents with pores in the range of 1.5–150 nm, thus revealing a porous character of the samples with a specific surface area of 191 m^2/g, average pore diameter of 158 Å and pore volume 0.5 cc/g. Average particle size, D_{BET} was 12 nm which have been confirmed by the BET isotherm. Hence BET isotherm and pore size distribution curve explains the presence of porosity in the nanoparticles which could have applications in gas adsorption and sensors.

TEM images of sol–gel derived nanocomposites are shown in Fig. 5. Non-homogeneous structures and selected

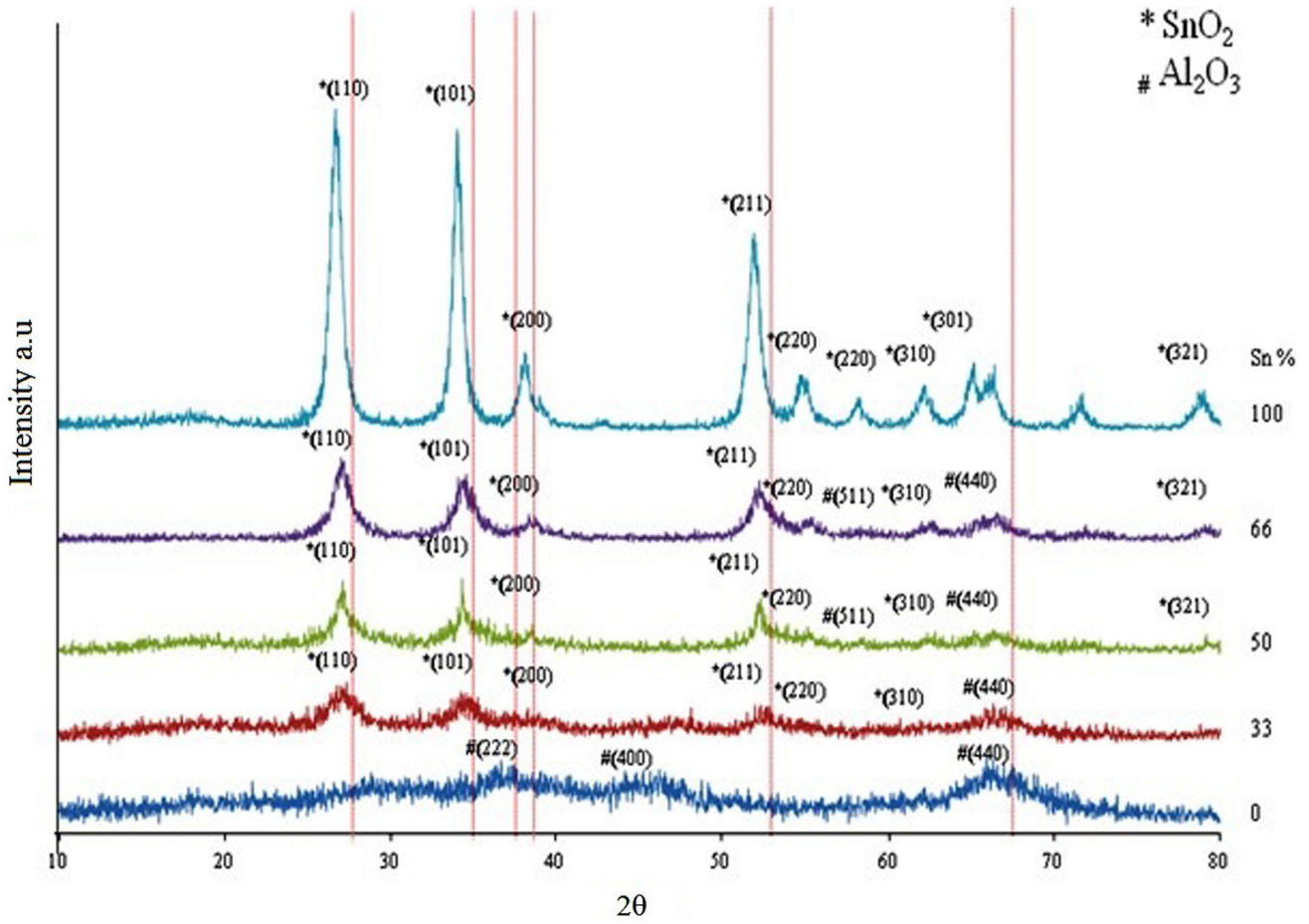

Fig. 1 Comparative XRD graph of all five $xSnO_2$–Al_2O_3 nanocomposites

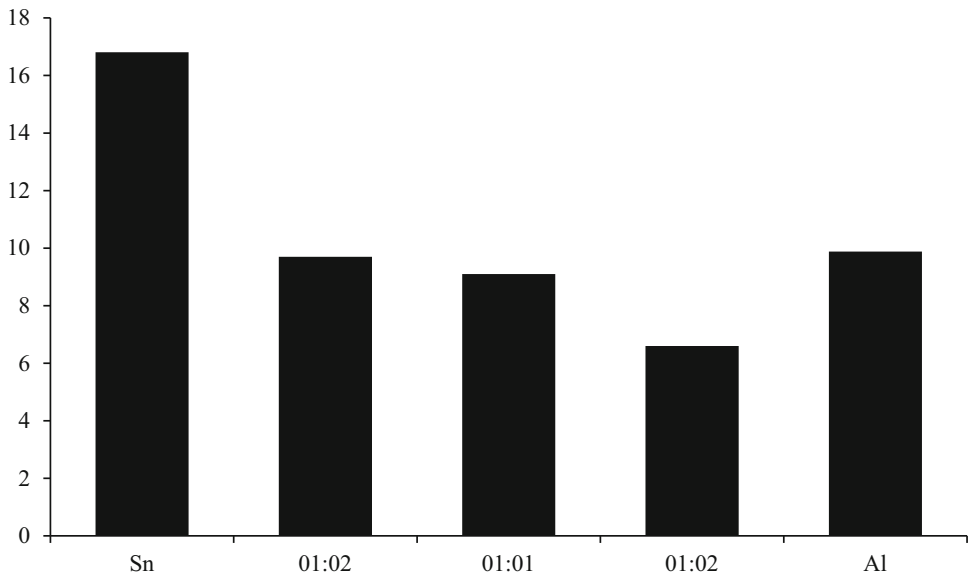

Fig. 2 Crystallite size of nanoparticles calculated by Debye-Scherer equation

area diffraction pattern is shown in inset of the Fig. 5, which indicates that the SnO_2–Al_2O_3 nanocomposites are highly crystalline in nature and the shape was found to be octagonal. It can be seen from the TEM image that the average particle size is 20–25 nm, which is in agreement with the crystallite, size obtained from XRD.

Table 1 Crystallite size of nanoparticles calculated by Debye-Scherer equation

S. No	Sn: Al ratio	Size (nm)
1	1:0	16.81
2	2:1	9.7
3	1:1	9.1
4	1:2	6.6
5	0:1	9.88

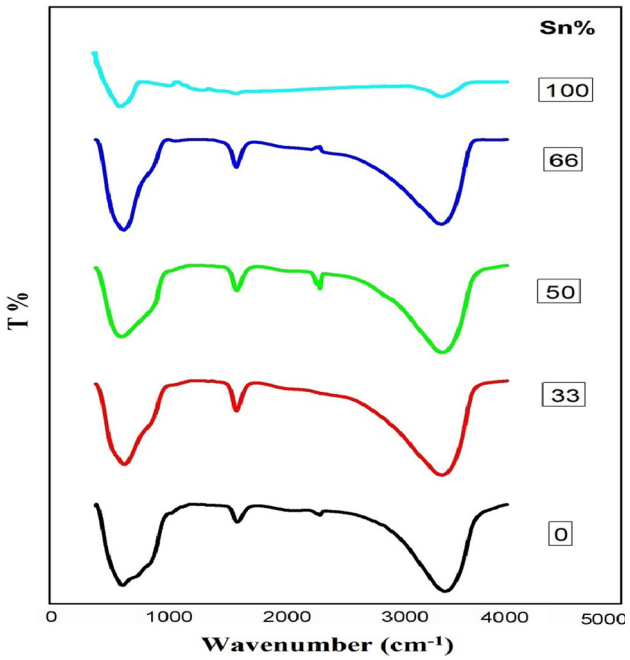

Fig. 3 FTIR spectra of $xSnO_2$–Al_2O_3 nanocomposites

Figure 6 shows the scanning electron micrographs (SEM) of SnO_2–Al_2O_3 nanocomposites at different magnifications in the 1 μm range as indicated by (a, b, c and d). It has been observed that nanocomposites exhibit spherical morphology and are highly porous, with foam-like structure clustering of particles seems to have occurred on the surface. The particle size measurement of SnO_2–Al_2O_3 nanocomposites from SEM images is found to be greater as compared to calculated from powder XRD. The increment in particle size of nanocomposites could be due to the sintering at 450 °C, resulting in particle binding and agglomeration (Ansari et al. 2002). However, SEM showed different aggregation of nano sized Al_2O_3 particles and there was a slight difference between particle size determination by the Scherrer method and particle size determination by SEM images due to particle binding and agglomeration. Although the scales that are shown in Fig. 6 (a, b, c and d) even then these appear to indicate formation of granular morphology, integrated by nanosized crystallites.

Table 2 shows energy disperse X-ray (EDX) spectroscopic analysis of SnO_2-Al_2O_3 nanocomposite. It shows that aluminium, tin and oxygen components are present in the nanocomposites, whereas chlorine and gold are also present in trace due to the impurities present in the commercially available precursor, which is also reported in the literature (Guzman et al. 2006). Hence it can be confirmed that the chemical composition should be SnO_2-Al_2O_3 which also agrees with the peaks of SnO_2 and Al_2O_3 in powder XRD spectra. Pure Al_2O_3 and pure SnO_2 exhibit their characteristics peaks i.e the amount of metal present is in proper agreement. EDX analysis indicates the presence of metal oxides in the relative composition ratio (SnO_2–Al_2O_3) of 1:0, 2:1, 1:1,1:2, 0:1.

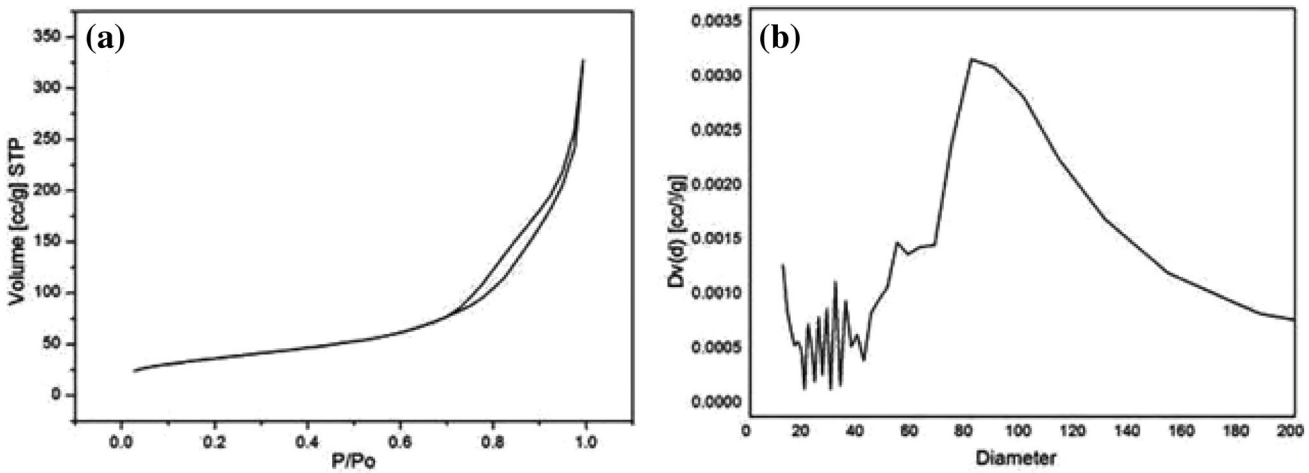

Fig. 4 **a** Nitrogen adsorption isotherms of .5 SnO_2–.5 Al_2O_3 nanocomposites. **b** Pore size distribution of .5 SnO_2– .5 Al_2O_3 nanocomposites

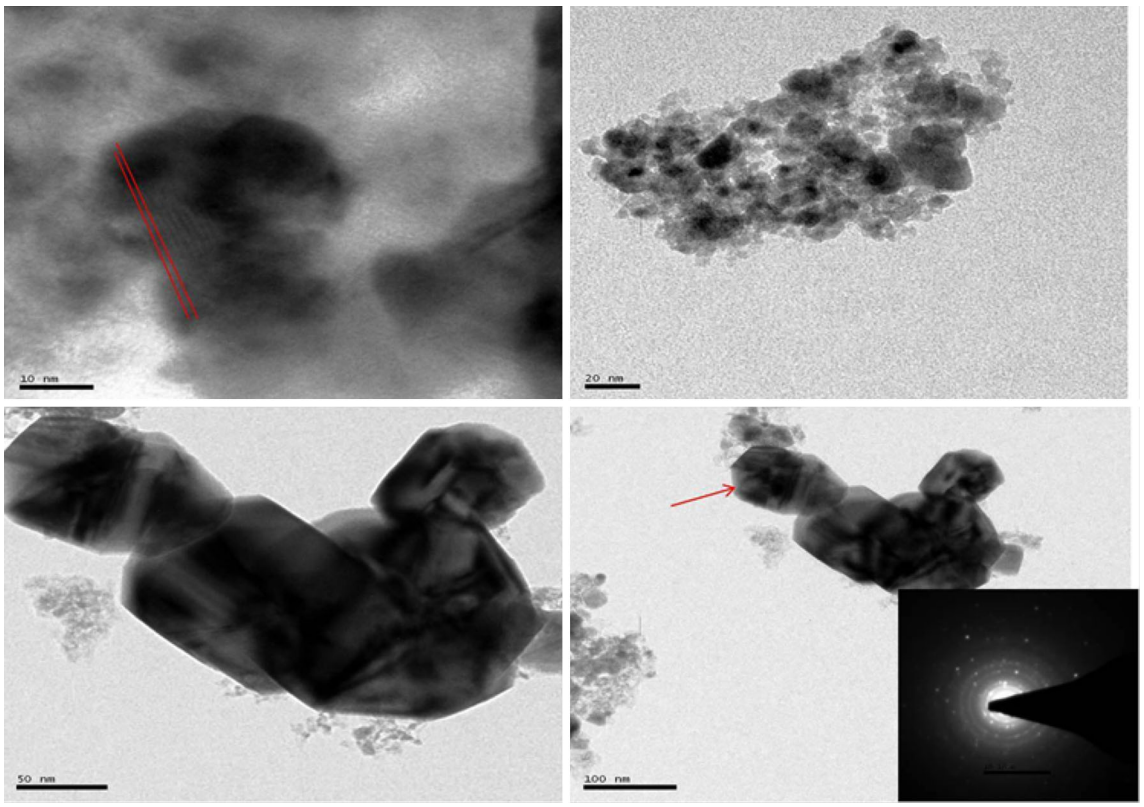

Fig. 5 TEM images of $xSnO_2$- Al_2O_3 nanocomposites synthesized via sol–gel route

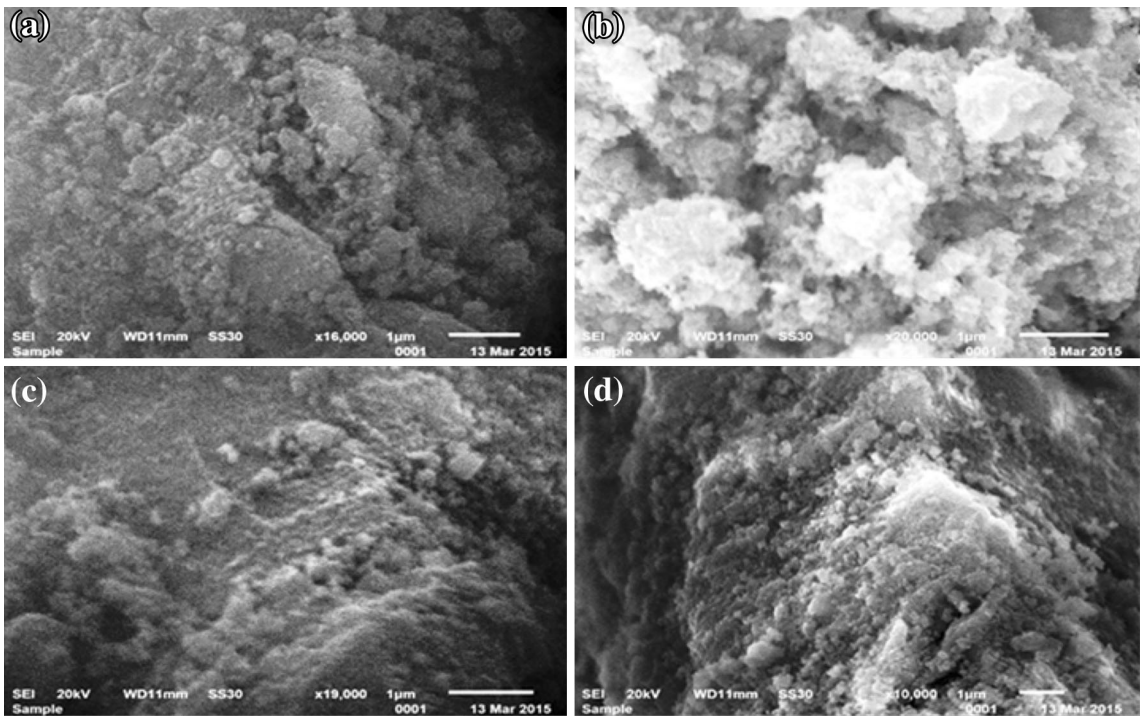

Fig. 6 SEM images of $xSnO_2$- Al_2O_3 nanocomposites synthesized via sol–gel route

Table 2 Chemical composition present in SnO_2- Al_2O_3 nanocomposites

S. No	Element	Weight (%)	Atomic (%)
1:0	O	8.87	41.37
	Sn	90.49	56.88
1:1	O	28.98	55.66
	Sn	37.3	28.1
	Al	33.72	28.8
1:2	O	31.16	52.26
	Sn	25.52	5.69
	Al	42.88	42.05
2:1	O	14.27	43.3
	Sn	70.60	9.31
	Al	15.57	37.03
0.1	O	45.62	58.62
	Al	45.29	41.37

Conclusion

Alumina Tin oxide nanocomposites with high surface area were synthesized through sol–gel route. The aluminium was entrenched in the SnO_2 lattice, interstitially forming a solid solution. The Brunauer–Emmett–Teller (BET) surface area successfully reached 191 m^2/g. N_2 adsorption characteristics revealed that they had pores of 15.8 nm or 158 Å, which contributed to the high surface area. Scanning electron microscopy, electron diffraction, and X-ray diffraction indicated the morphology, crystal structure, and chemical composition of nanocrystals. Novel process allowed us to avoid sintering and deformation of the crystals, and hence realized a high surface area and unique morphology.

Acknowledgments The work has been supported by University Grant Commission, New Delhi, India, Major Research Project F. No 42-286/2013 (SR). Authors would like to thank University Science Instrumentation Centre, University of Delhi, New Delhi, India for characterizations.

References

Adriana B, Claudia GR, Sergio RD, Osvaldo AS (2008) Use of Al_2O_3-SnO_2 as a support of Pt for selective dehydrogenation of light paraffins. Catal Today 133–135:28–34

Alcantara R, Fernandez-Madrigal FJ, Pıerez-Vicente C, Tirado JL, Jumas JC, Olivier-Fourcade Josette (2000) Preparation, sintering and electrochemical properties of tin dioxide and Al-doped tin dioxides obtained from citrate precursors. Chem Mater 12:3044–3051

Ansari A, Ansari SG, Ko T, Oh JH (2002) Effect of MoO_3 doping and grain size on SnO_2-enhancement of sensitivity and selectivity for CO and H_2 gas sensing. Sensor Actuat B-Chem 87:105–114

Aoki A, Sasakur H (1970) Tin oxide thin film transistors. Japan J Appl Phys 9:582

Buttà N, Cinquegrani L, Mugno E, Tagliente A, Pizzini S (1992) A family of tin oxide-based sensors with improved selectivity to methane. Sensor Actuat B-Chem 6:253–256

Chopra KL, Major S, Pandya DK (1983) Transparent conductors–a status review. Thin Solid Films 102:1–46

Granquist CG (1990) Window coatings for the future. Thin Solid Films 193:730–741

Guzman G, Dahmani B, Puetz J, Aegerter MA (2006) Transparent conducting sol–gel ATO coatings for display applications by an improved dip coating technique. Thin Solid Films 502:281–285

Heiba ZK, Ahmed MA, Ahmed MI (2010) Structural investigations of nanomixed oxides SnO_2–xAl_2O_3 prepared by sol–gel technique. J Alloy Compd 507:253–256

Jayalakshmi M, Venugopal N, Raja KP, Rao MM (2006) Nano SnO_2-Al_2O_3 mixed oxide and SnO_2–Al_2O_3 carbon composite oxides as new and novel electrodes for supercapacitor applications. J Power Sources 158:1538–1543

Kirszensztej P, Szymkowiak A, Martyla A, Marciniak P, Przekop R (2004) Porosity of aluminium oxide-based binary systems obtained by sol–gel method. React Kinet Catal Lett 82:287–293

Lopez T, Asomoza M, Bosch Garcia-Figueroa E, Gomez R (1992) Spectroscopic characterization and catalytic properties of sol–gel Pd/SiO_2 catalysts. J Catal 138:463–473

Lin C, Ritter JA, Amiridis MA (1997) Effect of thermal treatment on the nanostructure of $SiO_2.Al_2O_3$ xerogels. J Non-Cryst Solids 215:146–154

Ma LA, Ye Y, Hu LQ, Zheng KL, Guo TL (2008) Efficient field emission from patterned Al-doped SnO_2 nanowires. Physica E 40:3127–3130

Mandayo GG (2007) Gas Detection by Semiconductor Ceramics: Tin Oxide as improved Sensing Material. Sens Lett 5:341–360

Nakamura Y (1989) Stability of the sensitivity of SnO_2-based elements in the field. Chem Sen Tech 2:71–82

Niranjan RS, Hwang YK, Kim DK, Jhung SH, Chang JS, Mulla IS (2005) Nanostructured tin oxide, synthesis and gas-sensing properties. Mater Chem Phys 92:384–388

Peng Z, Shi Z, Liu M (2000) Mesoporous Sn–TiO_2 composite electrodes for lithium batteries. Chem Commun 21:2125–2126

Saha M, Banerjee A, Halder AK, Mondal J, Sen A, Maiti HS (2001) Effect of alumina addition on methane sensitivity of tin dioxide thick film. Sens Actuators B: Chem 79:192–195

Sheng TC, Lang S, Morrow BA, Gay ID (1994) Structure of SiO_2 and Al_2O_3 Monolayer Catalysts: Investigation by Infrared-Spectroscopy and ^{29}Si MAS NMR. J Catal 148:341–347

Sing KSW, Everett DH, Haul RKW, Moscou L, Pierotti RK, RouqueroI J, Siemieniewska T (1985) Reporting physisorption data for gas/solid systems with special reference to the determination of surface area and porosity. Pure App Chem 57:603–619

Venugopal Raja KP, Chakravarthi CK, Jayalakshmi M, Rao MM (2008) Synthesis of nanostructured SnO_2 dispersed on amorphous alumina by hydrothermal method. Mater Res Innov 12:127–133

Xu C, Tamaki J, Miura N, Yamazoe N (1991) Promotion of tin oxide gas sensor by aluminum doping. Talanta 30:1169–1175

Yamazoe N (1991) New approaches for improving semiconductor gas sensors. Sens Actuators B 5:7–19

Ying Z, Wan Q, Song ZT, Feng SL (2004) SnO_2 nanowhiskers and their ethanol sensing characteristics. Nanotechnology 15:1682–1684